

# Topological transformation of speckles by symmetry control and spiral wavefront modulation

Jérôme Gateau<sup>1</sup>, Ferdinand Claude<sup>2</sup>, Gilles Tessier<sup>2</sup>, and Marc Guillon<sup>2,\*</sup>

<sup>1</sup>Sorbonne Université, CNRS, INSERM, Laboratoire d’Imagerie Biomédicale, LIB, 15 rue de l’école de Médecine, F-75006, Paris, France

<sup>2</sup>Neurophotonics Laboratory, CNRS UMR 8250, Paris Descartes University, Sorbonne Paris Cité, Paris, France

\*Corresponding author: marc.guillon@parisdescartes.fr

December 20, 2024

**Deterministic control of coherent random light typically requires prior characterization of the generating diffuser. Only a few simple speckle transforms can be achieved by blind wavefront modulation of the impinging beam. Recently, it was shown that spiral phase modulation results in a permutation of intensity maxima and intrinsic  $\pm 1$ -charged optical vortices. Here, this cyclic-group algebra is analyzed when combining spiral phase transforms of charge  $n$  with star-like amplitude modulation masks exhibiting point-group symmetry  $D_3$  and  $D_4$ . This combination allows statistical strengthening of permutations and controlling the period to be 3 and 4, respectively. Phase saddle-points are shown to complete the cycle.**

## 1 Introduction

The propagation of coherent light through scattering media yields random wavefields with typical intensity structures called optical speckles. The control of light distribution inside and through complex media by wavefront modulation of the impinging beam is of critical importance for application ranging from bio-imaging [1] to telecommunications [2]. Information transmission through diffusers is typically characterized in terms of field and intensity correlations [3]. For diffusers exhibiting so-called “memory effect” correlations, important invariants were identified under specific spatial (tilt and shift) transformations [4, 5, 6, 7]. Additionally, regardless of the wavefront of the impinging beam, critical points in random wavefields exhibit many topological correlations [8], which thus demand the development specific tools to be analyzed. Optical vortices are especially important critical points since they are centered on singular phase points coinciding with nodal points of the intensity. They spontaneously appear in random wavefields [9], and thereby allow efficient super-resolution microscopy [10, 11]. The present work aims at exploring the possibility to manipulate topological correlations

between critical points in random wavefields under symmetry control and spiral wavefront modulation, in a Fourier plane of the impinging beam.

Critical points are characterized by their topological charge and their Poincare number [12]. They may typically be controlled by applying phase or amplitude masks in a Fourier plane. Any smooth and regular transform of the wavefield (either in phase or amplitude) induces changes preserving both the topological charge and the Poincare number [8, 13]. Noteworthy, these conservation rules account for the topological stability of isolated vortices of charge 1 in speckles since the creation or annihilation of vortices can only occur by pairs [13, 10]. As opposed to smooth phase transforms, the addition of a spiral phase mask in a Fourier plane is a *singular transform* and results in a change of the total orbital angular momentum [14, 15]. Recently, considering correlations between the spatial distribution of critical points in a speckle under such spiral phase transforms [16], we observed a strong inter-play between intensity maxima and optical vortices. More precisely, the obtained results suggested that the topological charge of these critical points were all incremented by applying a  $+1$  spiral phase mask in the Fourier plane. The impossibility to spontaneously get  $+2$ -charged vortices (unstable and thus unlikely in random light structures [17]) resulted in the observation of a partial cyclic permutation of the three populations of critical points (namely, maxima and  $\pm 1$ -charged vortices). Furthermore, as a third kind of possible transform, it was observed that the orbital angular momentum may be not conserved when using amplitude masks with a high degree of symmetries [18, 19]. As a result, optical vortices can be created using simple amplitude masks [20, 21]. This property proved to be of interest for imaging applications to reveal symmetries of an imaged object [22, 23, 24] and for allowing topological charge measurements [25], especially in astronomy [26].

Here, combining spiral phase transforms of order  $n$  with star-like amplitude masks having discrete point group symmetries  $D_3$  and  $D_4$ , we study experimentally the topological

correlations between intensity maxima and optical vortices in speckles. A new co-localization criterion is proposed, inspired by statistical mechanics. Although random wavefields do not possess any symmetry, such a combination allows us to strengthen periodicity and even to control the period of the cyclic permutation. Noteworthy, for an amplitude mask of symmetry  $D_4$ , a phase saddle point appears as a complementary critical point to complete a cycle of period 4. A transposition between  $V^+$  and  $V^-$  is also revealed when adding a 2-charged spiral phase mask.

## 2 Experimental procedure

The experimental procedure consisted in modulating a random phase pattern in a Fourier plane with an amplitude mask and a spiral phase mask. Here, spiral phase masks of order  $n$ ,  $SP_n(\theta) = e^{i \cdot n \cdot \theta}$  (in polar coordinates), were applied for  $n \in \llbracket -6; 6 \rrbracket$ . As amplitude masks, three Binary Amplitude (BA) masks were used: a disk and two periodic angular slits with a point group symmetry  $D_3$  and  $D_4$ . They are defined by the following angular transmission function (in polar coordinates):

$$BA^N(\theta) = \begin{cases} 1, & \text{if } |\theta - (k - \frac{1}{2}) \cdot \frac{2\pi}{N}| < \frac{\pi}{32} \text{ with } k \in \llbracket 1; N \rrbracket \\ 0, & \text{otherwise.} \end{cases} \quad (1)$$

for  $N \in \{3, 4\}$ . By convention,  $BA^\infty$  defines the disk-shaped aperture (obtained for  $N \geq 32$ ). For  $N < 32$ , the orbital angular momentum content (or spiral spectrum [27]) of the  $BA^N$  aperture exhibits discrete harmonics for the spiral modes  $n = p \cdot N$  with  $p \in \mathbb{Z}$ . Given the width of the angular slits and provided that  $N=3$  or  $4$ , the aperture  $BA^N$  can be considered as invariant by the addition of  $SP_n$  when  $n = \pm N$  or  $\pm 2 \cdot N$ . Such an invariance in the Fourier plane is thus necessarily associated with a periodic transform of the speckle pattern in the real space.

The experimental configuration is detailed in Fig. 1. A spatial light modulator (SLM) (LCOS, X10468, Hamamatsu) was illuminated with a collimated laser beam at 635 nm and Fourier conjugated to a camera (768x1024 pixels) with a converging lens. The phase  $\Phi_n$  and amplitude  $A_n$  of the modulated ( $SP_n$  mask) random wave were measured at the camera plane by phase stepping interferometry. To do so, the SLM was split in two parts to generate both the modulated random wave (or signal wave) on one side and a reference wave on the other side (see Fig. 1a). The signal wave was generated by adding simultaneously the scattering random phase pattern, the spiral phase modulation  $SP_n$  and the amplitude mask  $BA^N$ . Adding a blazed grating achieved spatial separation of the imprinted signal wavefront from undiffracted light (the latter being sent to a beam-block). The signal speckle intensity  $I_n$  could be measured directly by removing the contribution of the reference beam.

For phase-stepping interferometry, an additional Fresnel lens was added to the reference beam in order to cover the camera surface. The latter spherical contribution as well as

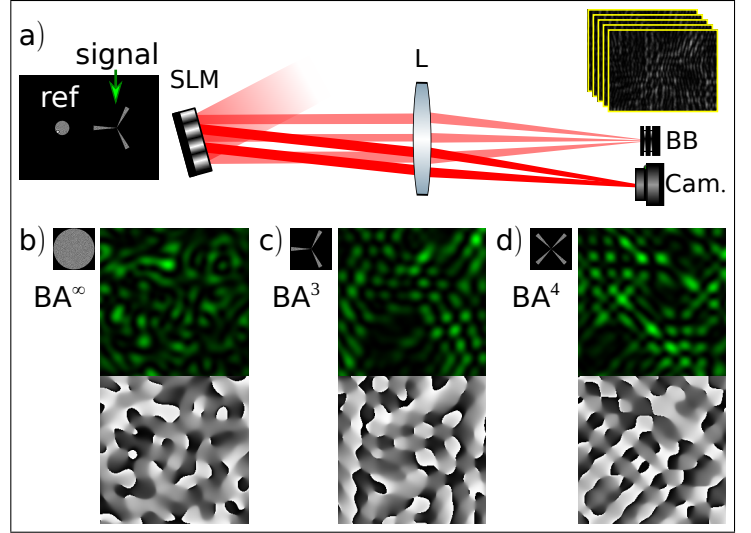


**Fig. 1:** Experimental setup (a) used to measure the intensity and the phase of speckle patterns corresponding to the different binary amplitude masks. A spatial light modulator (SLM) is illuminated with a collimated laser beam at 635nm. The phase is measured by phase stepping interferometry. Both the reference and the signal wavefronts are imprinted on the SLM. In addition to a blazed grating which allows sending undiffracted light to a beam block (BB) and the first order diffracted beam to a camera (Cam.). A stack of eight images was then sequentially recorded while phase shifting the reference beam. The measured intensity  $I_0$  maps (top, green colorscale) and phase  $\Phi_0$  maps (bottom, gray colorscale) are presented for (b) a circular aperture ( $BA^\infty$ ), (c) periodic angular-slits with a point group symmetry  $D_3$  ( $BA^3$ ), and (d) periodic angular-slits with a point group symmetry  $D_4$  ( $BA^4$ ). Miniatures of the BA masks are displayed for illustration.

the relative phase-tilt between the signal and the reference beams were removed in a numerical post-processing step. A stack of eight images was sequentially recorded by phase shifting the reference beam by  $2\pi/9$  phase-steps. All BA masks had the same radius of  $r = 170$  pixels at the SLM, so yielding the same speckle grains size on the camera plane:  $\lambda/(2NA)$ -Full Width Half Maximum (FWHM), where  $\lambda$  is the wavelength and  $NA \simeq r/f$  the numerical aperture of illumination (with  $f = 750$  mm the focal length of the lens L in Fig. 1a). The BA radius  $r$  was set in order to have a speckle grain size of 15 camera pixels. Hereafter, all distances and spatial densities are expressed setting  $\lambda/(2NA)$  as the length unit.

In Fig. 1(b-d), an illustration of the speckle intensity and phase maps obtained for the three different geometries of BA masks is shown. In the following study, intensity maps  $I_n$  and phase maps  $\Phi_n$  were measured for all three  $BA^N$  masks ( $N \in \{3, 4, \infty\}$ ) and for each  $SP_n$  masks ( $n \in \llbracket -6; 6 \rrbracket$ ). For comparison, the intensity-map  $I_{\text{rand}}$  and the phase-map  $\Phi_{\text{rand}}$  obtained for a non-correlated scattering random pattern were acquired for all the  $BA^N$  masks independently.

### 3 Statistical analysis of the topological correlation between critical points

#### 3.1 Studied critical points

The field at the camera being linearly polarized, optical fields are here studied as scalar fields. The location of the main critical points of the experimental intensity and phase maps were measured and their statistical correlation distances were analyzed. Importantly, for a given BA mask, adding  $SP_n$  masks preserves all statistical properties of the speckle patterns, such as the number-density of critical points. Phase saddle-points of  $\Phi_n$  are notated  $S_n^p$  and vortices of charge  $\pm 1$ :  $V_n^\pm$ . Vortices of charge higher than 1 do not appear in Gaussian random wavefields [17]. Maxima and saddle-points of  $I_n$  are notated  $M_n$  and  $S_n^I$ , respectively. Non-zero minima and phase extrema have not been considered here, since having significantly lower densities [28]. All the notations are summarized in Table 1.

The measured average number-densities of the critical points are presented in Table 2. The density of the critical points of type  $X$  ( $X = V^\pm, M, S^p$  or  $S^I$ ) is notated  $\rho(X)$ . As expected,  $\rho(V^-)$  and  $\rho(V^+)$  are equal [8], and  $\rho(X)$  depends both on the type of critical point and the BA mask.

Table 1: Notations for the main critical points

Phase	Maxima	Saddle	Vortices (charge $\pm 1$ )
	-	$S^p$	$V^-$ and $V^+$
Intensity	Maxima	Saddle	Zeros
	$M$	$S^I$	$V^-$ and $V^+$

Table 2: Measured average number density of critical points (length unit:  $\lambda/(2\text{NA})$ ). The average number of  $V^-$  is 660.85 for the circular aperture ( $BA^\infty$ ).

BA mask	$V^-$ (or $V^+$ )	$M$	$S^p$	$S^I$
$BA^\infty$	0.19	0.32	0.36	0.65
$BA^3$	0.20	0.39	0.36	0.79
$BA^4$	0.19	0.33	0.40	0.70

#### 3.2 Statistical tools for the analysis of topological correlations

To study statistical transformations of critical points quantitatively, new specific tools are presented. What we discuss as transformation of critical points by the addition of spiral phase masks refers to the mean nearest neighbor distances between populations of critical points and calls for a discrimination parameter. Two specific statistical tools are then described below: the radial density function (RDF) and the Weighted Median Normalized Distance (WMND).

In our previous study [16], correlations between critical points could be characterized by computing the radial proba-

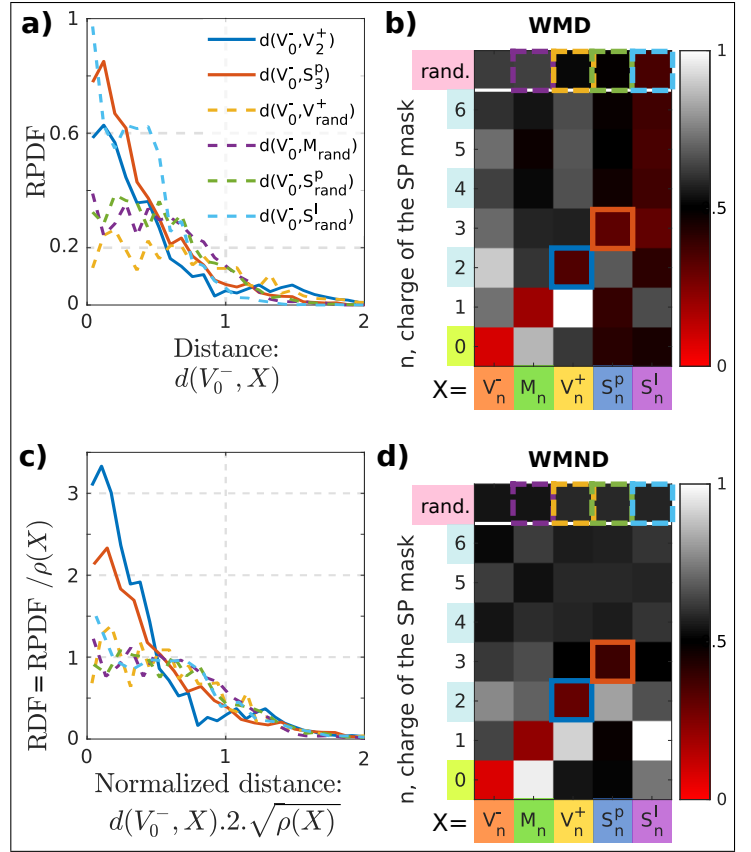


**Fig. 2:** Statistical analysis of the separation distances between one set of critical points (here  $V_0^-$ ) and the closest point of another set (notated  $X$ ). The distance between  $V_0^-$  and the closest  $X$  is notated  $d(V_0^-, X)$ . The Radial Probability Density Functions (RPDF) of the nearest neighbor (a) and the corresponding Weighted Median Distance (WMD) (b) are shown. Radial Distribution Functions (RDF) of the nearest neighbor (c) and the corresponding Weighted Median Normalized Distance (WMND) (d) provide a statistical toolbox to study the spatial correlation between pairs of critical points. The results were derived from experimental measurements of  $I_n$  and  $\Phi_n$  obtained for the amplitude mask  $BA^\infty$ .

bility density function (RPDF) of the nearest-neighbor distance. Fig. 2a presents RPDFs of the distance  $d(V_0^-, X)$  in the case of  $BA^\infty$ . We define  $d(Y, X)$  as the distance between a  $Y$ -point and the closest  $X$ -point. The RPDF( $r$ ) corresponds to the probability to find the closest  $X$ -point at the distance  $r$  from a  $Y$ -point, per unit area. One drawback associated with the use of the RPDF is that it may suggest paradoxes if improperly interpreted. Considering  $d(V_0^-, V_2^+)$  and  $d(V_0^-, S_{rand}^I)$ , it seems that  $V_0^-$  correlates both with  $V_2^+$  and  $S_{rand}^I$  since both RPDFs reach high values at zero distances. While a correlation is expected in the former case (due to topological charge incrementation), no correlation is expected from the latter which involves two independent sets of random points. The reason why the amplitude of the RPDF of  $d(V_0^-, S_{rand}^I)$  is higher than the one of  $d(V_0^-, V_2^+)$  at zero distances, is just due to the  $\sim 3$ -times higher spatial density

of intensity saddle points  $S_{\text{rand}}^I$  as compared to vortices  $V_2^+$  (see Table 2): the probability to find a saddle point at close distance is thus larger. To quantitatively characterize topological correlations, we thus need to normalize RPDFs by the number densities  $\rho(X)$ .

Our first statistical tool, the radial-distribution function (RDF) – well known in statistical mechanics [29] – was extended here for nearest neighbor by normalizing the RPDF of  $d(V_0^-, X)$  by  $\rho(X)$ , and the distances  $d(V_0^-, X)$  by the mean X-interpoint half-distance  $(2\sqrt{\rho(X)})^{-1}$  [30]. Fig. 2c shows the RDF of the same data as in Fig. 2a. As a result, all the RDFs of  $d(V_0^-, X_{\text{rand}}) \cdot 2\sqrt{\rho(X)}$  are superimposed for every  $X_{\text{rand}}$ , and the spatial correlation between  $V_0^-$  and  $V_2^+$  clearly appears.

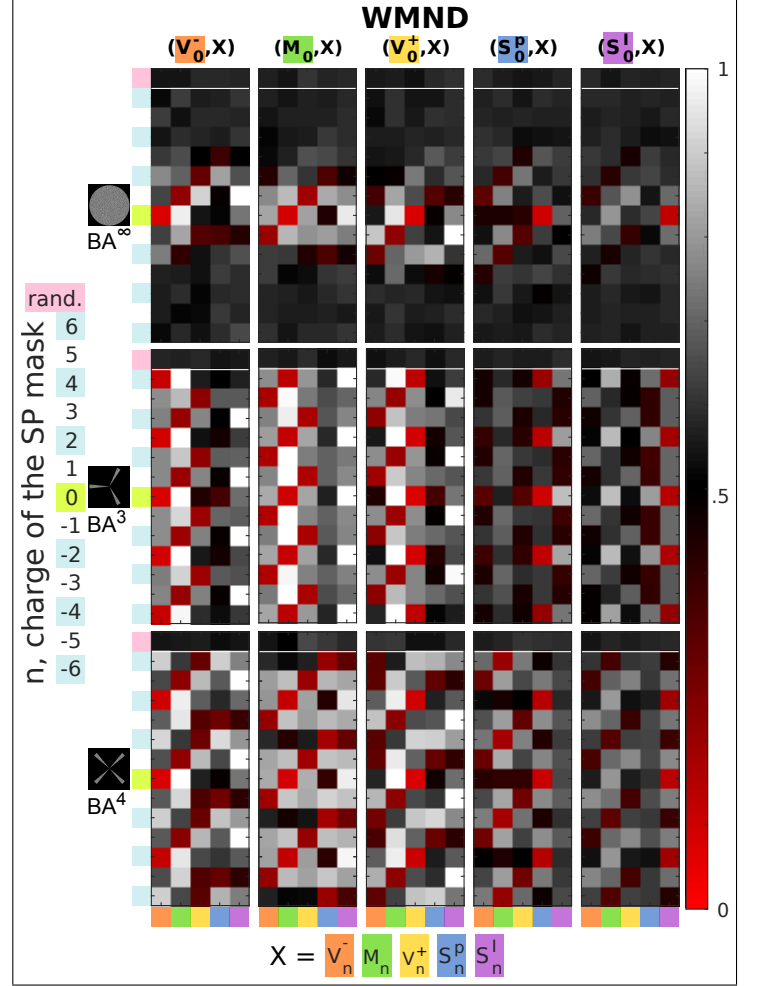
To obtain a single binary parameter discriminating the spatial correlation between  $V_0^-$  and  $X$ , we further define the Weighted Median Normalized Distance (WMND) as a second statistical tool: the  $\text{WMND}(V_0^-, X)$  is the 50% weighted percentile of  $d(V_0^-, X) \cdot 2\sqrt{\rho(X)}$  with weights corresponding to the RDF values. A  $\text{WMND}(V_0^-, X)$  around 0.5 means that no spatial correlation exist between  $V_0^-$  and  $X$ , while  $\text{WMND} < 0.5$  and  $\text{WMND} > 0.5$  mean an attraction and a repulsion, respectively. A zero WMND value means perfect correlation while  $\text{WMND}=1$  means perfect anti-correlation.

Fig 2d presents the  $\text{WMND}(V_0^-, X)$  for all the critical points considered in this study and for  $n \in \llbracket 0; 6 \rrbracket$ . For comparison, the Weighted Median Distance (WMD) associated with the RPDFs – defined as the 50% weighted percentile of  $d(V_0^-, X)$  with weights corresponding to the RPDF values – is also computed and displayed in Fig. 2b. To validate this tool, taking  $BA^\infty$  as an illustrative example, we notice that  $\text{WMND}(V_0^-, X_{\text{rand}})$  is around 0.5 for all the  $X_{\text{rand}}$ , as expected. By comparison,  $\text{WMD}(V_0^-, S_{\text{rand}}^I) = 0.35$ , which irrelevantly suggests correlations as discussed above. Moreover, for  $n > 3$ , the RDFs of  $d(V_0^-, X_n)$  are observed to match the RDFs of  $d(V_0^-, X_{\text{rand}})$ : no noticeable spatial correlation is obtained for  $n > 3$ . As expected again, the  $\text{WMND}(V_0^-, X_{\text{rand}})$  are around 0.5 for  $n > 3$ . Conversely, we get  $\text{WMD}(V_0^-, S_n^I) < 0.38$ , which would falsely suggest correlations. All these observations validate the WMND as a parameter to assess the spatial correlation between pairs of critical points in a speckle pattern.

## 4 Topological correlations between critical points for the different amplitude masks

Fig. 3 presents the  $\text{WMND}(Y_0, X_n)$  for all the critical points ( $Y_0$  and  $X_n$ ) screened in this study, for  $SP_n$  masks with  $n \in \llbracket -6; 6 \rrbracket$  and for the three considered BA apertures. The WMND was verified to be around 0.5 for all the amplitude masks and all the pairs  $(Y_0, X_{\text{rand}})$ , for which there is obviously no spatial correlation. For the sake of readability, in the following, we only discuss the interplay between critical

points when adding positively charged SP masks but symmetrical behaviours are observed for negatively charged SP masks (Fig. 3).



**Fig. 3:** Weighted Median Normalized Distance (WMND) for all possible pairs of critical points screened here and for the addition of spiral phase mask with charges up to  $n = \pm 6$ . The WMND were computed from experimental measurements of  $I_n$  and  $\Phi_n$ .

For the aperture  $BA^\infty$ , the WMND reveals several noticeable features (reported in Table 3). First, as expected from our previous study [16], we notice some spatial correlations for the triplets  $(V_{m-1}^-, M_m, V_{m+1}^+)$ . Because  $\rho(V_0^-) < \rho(M_1)$ , a one-to-one transformation is impossible between vortices and maxima. Although  $V_0^-$  and  $V_2^+$  have the same number density, we also notice that  $\text{WMND}(V_0^-, V_2^+)$  is significantly different from 0, indicating that the rate of the macroscopic transformation from  $V_0^-$  to  $V_2^+$  is below 1.

In agreement with the 3-point cyclic permutation algebra observed in [16], a weak attraction is found for the pair  $(V_0^+, V_{+1}^-)$ , corresponding to the topological-charge equation  $1+1 = -1$ . However, as an alternative transformation for  $V_0^+$ , a similar attraction is now also observed for  $(V_0^+, S_{+1}^p)$ .  $V_0^+$  is thus subject to a bifurcation between  $V_{+1}^-$  and  $S_{+1}^p$ , which

implies two different mechanisms.

As a first possibility, some  $V_0^+$  transform into  $S_{+1}^p$ . This transformation inspires the following interpretation: When adding a  $SP_{+1}$  phase mask to an isolated Laguerre-Gaussian beam with topological charge +1, a +2-charged vortex is obtained. Under weak perturbation, this +2 vortex splits into two +1 vortices, accompanied by the creation of both an intensity and a phase saddle point in between [13]. The creation of this pair of saddle points is governed by the Poincaré number conservation. In the frame of this model, a  $V_0^+$  vortex is expected to co-localize with both  $S_{+1}^I$  and  $S_{+1}^p$  and to anti-correlate with the two  $V_1^+$  that split away. Although no noticeable spatial attraction was found for  $(V_0^+, S_{+1}^I)$ , a co-localization is observed for  $(V_0^+, S_{+1}^p)$  and a weak repulsion is observed for the pair  $(V_0^+, V_{+1}^+)$ , consistent with this interpretation. In speckles, where +2-charged vortices cannot be encountered since unstable [17], the weak perturbation approximation cannot be fully valid, potentially accounting for the remaining discrepancy between experimental observations and the proposed model.

As a second possible transformation, the more surprising attraction of the pairs  $(V_0^+, V_{+1}^-)$  is observed, which calls for another mechanism. Since no such transformation can be imagined from isotropic  $V_0^+$ , it may only be interpreted by a mechanism dominated by strong perturbations. The statistically uniform mesh created by vortices and maxima in speckles [31], together with strong correlations observed for pairs  $(M_0, V_{+1}^+)$  and  $(V_0^-, M_1)$  seem to constrain  $V_0^+$  to co-localize with  $V_{+1}^-$ . This transformation would deserve further analytical investigation but we anticipate that the creation mechanism of  $V_{+1}^-$  from  $V_0^+$  can only be a many-body problem, involving the field structure (maxima, phase saddles and vortices) surrounding the initial  $V_0^+$  of interest.

When adding a  $SP_{+2}$  mask for  $BA^\infty$ ,  $V_0^+$  is not observed to significantly co-localize with any remarkable critical point (see Fig. 3 and Table 3), whereas two possible transformations might have been expected for  $V_0^+$ . On the one hand, from the 3-point cyclic permutation, we could expect that  $V_0^+$  would transform into  $M_{+2}$ . On the other hand, since in Table 3, maxima and phase saddle-points are noted to be simply exchanged (see pairs  $(M_0, S_{+2}^p)$  and  $(S_0^p, M_{+2})$ ), a similar symmetrical exchange between -1 and +1 vortices could be expected, yielding a transformation of  $V_0^+$  into  $V_2^-$  (as  $V_0^-$  is transformed into  $V_2^+$ ). However, no such correlation is observed either for the pair  $(V_0^+, M_2)$  or for  $(V_0^+, V_2^-)$ . Conversely, these correlations appear when applying amplitude masks  $BA^3$  and  $BA^4$ , respectively, as detailed in the following.

For  $|n| > 3$ , no significant spatial correlation with the addition of  $SP_n$  is observed for  $BA^\infty$ . This aperture has a circular symmetry. Therefore, its spiral spectrum contains only the fundamental spiral mode  $n = 0$ , and is not invariant by the addition of any SP masks. All the described topological correlations associated with  $BA^\infty$  are summarized in Table 3.

As a possible solution to strengthen the 3-point cyclic permutation, we used the  $BA^3$  amplitude mask, making the Fourier plane almost invariant with respect to the addition of

Table 3: **Macroscopic transformations observed for the critical points  $Y_0$  with the amplitude mask  $BA^\infty$ . The transformation rates are below 1.**

Crit. point $Y_0$		Add. $SP_{+1}$		Add. $SP_{+2}$
$V_0^-$	$\rightarrow$	$M_1$	$\rightarrow$	$V_2^+$
$M_0$	$\rightarrow$	$V_1^+$	$\rightarrow$	$S_2^p$
$V_0^+$	$\rightarrow$	$V_1^- + S_1^p$	$\rightarrow$	$\emptyset$
$S_0^p$	$\rightarrow$	$V_1^-$	$\rightarrow$	$M_2$
Add. $SP_{-2}$		Add. $SP_{-1}$		Crit. point $Y_0$
$\emptyset$	$\leftarrow$	$V_{-1}^+ + S_{-1}^p$	$\leftarrow$	$V_0^-$
$S_{-2}^p$	$\leftarrow$	$V_{-1}^-$	$\leftarrow$	$M_0$
$V_{-2}$	$\leftarrow$	$M_{-1}$	$\leftarrow$	$V_0^+$
$M_{-2}$	$\leftarrow$	$V_{-1}^+$	$\leftarrow$	$S_0^p$

$SP_{\pm 3k}$  (so long as  $3k$ , with  $k$  integer, remains small enough). Here, four main observations can be noted. First, as expected, the pairs  $(Y_0, Y_{\pm 3})$  and  $(Y_0, Y_{\pm 6})$  are observed to have a WMND very close to zero, indicating that the macroscopic transformation rate is close to 1 for all these pairs. Second, we observe that the cycle of period 3 reinforces the spatial correlations of the triplet  $(V_{m-1}^-, M_m, V_{m+1}^+)$  and even extends it to the 3<sup>rd</sup> and 6<sup>th</sup> spiral harmonics. Third, no noticeable correlation is observed between  $V_0^+$  and phase saddle-points  $S_{+1}^p$  (although an anti-correlation is obtained between  $V_0^+$  and  $V_{+1}^+$ ), contrary to the case of  $BA^\infty$ . The periodicity of 3 induces a strong correlation for the pairs  $(V_0^+, V_{+1}^-)$ , and establishes a cyclic permutation of three populations of critical points  $V^-$ ,  $M$  and  $V^+$ . Forth, as a consequence, the pairs  $(V_0^+, M_2)$  also exhibit strong spatial correlations, contrary to the case of  $BA^\infty$ . In these two latter permutations, it must be reminded that not all intensity maxima  $M$  may transform into vortices, because of the difference in spatial densities (Table 2) of these two populations of critical points [16].

Next, we constrained the period to be equal to 4 by using the  $BA^4$  mask. In this case, the  $WMND(Y_0, Y_{\pm 4})$  are close to zero (transformation rate close to 1). As expected, this periodicity enhances the spatial correlation for the quadruplet  $(V_{m-1}^-, M_m, V_{m+1}^+, S_{m+2}^p)$  and extends it to their 4<sup>th</sup> spiral harmonics. Furthermore, in Fig. 3, strong correlations are observed for the pairs  $(V_0^-, M_1)$ ,  $(M_0, V_{+1}^+)$  and  $(S_0^p, V_{+1}^-)$ . However,  $V_0^+$  is still observed to bifurcate between  $V_{+1}^-$  and  $S_{+1}^p$  with the same likelihood, similarly to the  $BA^\infty$  case. Therefore the cyclic permutation of four populations of critical points  $S^p$ ,  $V^-$ ,  $M$  and  $V^+$  is not clearly established for  $BA^4$  (conversely to the permutation obtained for  $BA^3$ ).

When considering the addition of  $\pm 2$ -charged spiral masks for  $BA^4$ , a transposition (2-cycle permutation) between  $V^+$  and  $V^-$  is clearly obtained (with a transposition rate below 1). A strong spatial correlation, reinforced as compared to  $BA^\infty$ , is also clearly observed between  $M$  and  $S^p$  by addition of  $SP_{\pm 2k}$ .

In summary, the results displayed in Fig. 3 reveals the fundamental topological transformations of critical points in a speckle with the addition of SP mask for a single-spiral



mode aperture ( $BA^\infty$ ), and demonstrate the possible modification of topological transformation by the addition of BA masks with dihedral symmetry. For the sake of simplicity, we chose here star-like amplitude masks with a dihedral symmetry which comprise spiral harmonics with equal amplitudes (at small enough spiral mode number).

## 5 Wavefield control in the vicinity of critical points

On a local scale, the transformations of critical points shown in Fig. 3 arise from the convolution in the imaging plane of the scattered field with the point spread function (PSF) associated with the combined amplitude and spiral phase masks. Controlling the transformation of a critical point  $Y_0$  of the complex wavefield  $A_0$ , by adding a  $SP_n$  mask ( $n \in \mathbb{Z}^*$ ) in a Fourier plane, requires that the PSF associated with the combination of the  $SP_n$  and BA masks has a significant amplitude in the coherence area surrounding the critical point, or in other words: the area where the randomness of the speckle pattern has a limited influence as compared to the control by the incident wavefield. As a definition for the coherence area, we use the one proposed by Freund [32]:  $C_{area} = (\rho(V^+) + \rho(V^-))^{-1}/2$ . This definition avoids issues related to the shape of the aperture [32] encountered when considering the area of the intensity autocorrelation peak [33]. In our case, for all three BA masks, the coherence length was measured to be:  $C_{length} = \sqrt{C_{area}} \simeq \lambda/(2.NA)$ .

Experimentally, the PSFs can be obtained (Fig. 4a) by computing the intensity cross-correlations of the measured speckle pattern  $I_0$  and the measured speckle patterns  $I_n$  associated with  $SP_n$  masks ( $n \in \llbracket 0; 6 \rrbracket$ ) and for the three BA masks. The mean values of  $I_n$  were subtracted before computing the cross-correlations. The intensity cross-correlations  $xcorr(I_0, I_n)$  are identical to the PSF of the combined BA and  $SP_n$  masks. The centered spot of the autocorrelation  $xcorr(I_0, I_0)$  illustrates the spatial extent of the coherence area, and has the same dimension for all three BA masks since having the same radial aperture.

For  $BA^\infty$ , we observe that  $xcorr(I_0, I_n)$  has a circular symmetry with the highest values distributed on a ring whose radius (marked with a green line) increases with  $n$  (Fig. 4b), as observed for simple Laguerre-Gaussian beams [34]. Interestingly, for  $n > 3$ , not only we observe that the ring radius is larger than twice  $C_{length}$  but also that its amplitude is decreased to below 1/10 of the auto-correlation peak value (Fig. 4c). As a consequence, the transformation of critical points by applying  $SP_n$  masks is inefficient (or “unlikely”) and dominated by the surrounding random field. For this reason, no spatial correlation between pairs of critical points ( $Y_0, X_n$ ) could be found for  $n > 3$ . For  $BA^3$  and  $BA^4$ , the cross-correlation patterns  $xcorr(I_0, I_n)$  have dihedral symmetries  $D_3$  and  $D_4$  and a periodicity of  $N = 3$  and 4, respectively. In both cases, the radial distance of the strongest peak remains below  $1.4 * C_{length}$ , and its amplitude always remains above 1/3 of the auto-correlation maximum value (Fig. 4c).

The addition of the  $SP_n$  mask thus allows controlling the field inside the coherence area surrounding critical points  $Y_0$ , even for  $n > 3$ .

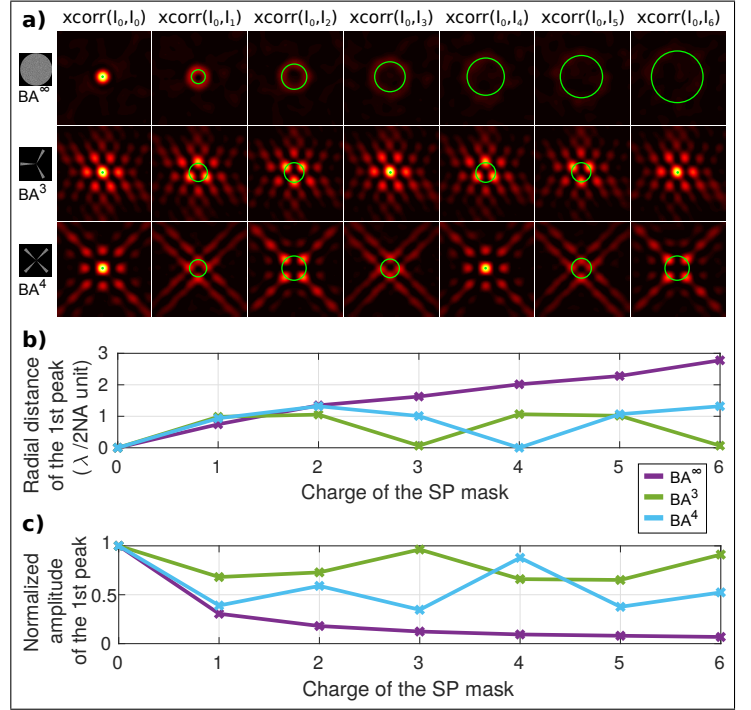


**Fig. 4:** Cross-correlation (a) of the speckle patterns  $I_0$  and  $I_n$  with  $n \in \llbracket 0; 6 \rrbracket$ . The cross correlations illustrate the spatial distribution of the intensity in the point spread function associated with the combined amplitude and spiral phase masks. The colorscale set for the autocorrelations  $xcorr(I_0, I_0)$  and was kept for the intercorrelations  $xcorr(I_0, I_n)$ . A N-periodicity is observed for the aperture  $BA^N$  with  $N = 3$  or 4. Green circles mark the radial distance to the strongest peak. (b) Radial distance and (c) normalized amplitude of the strongest peak as a function of the charge of the spiral phase mask. The radial distance keeps increasing for the circular aperture  $BA^\infty$  while it remains close or below  $\lambda/(2.NA)$  (the coherence length of the speckle) even for  $SP_n$  with  $n \geq 3$  for the aperture  $BA^N$  and  $N = 3$  or 4. The amplitude decreases for  $BA^\infty$  while it remains above 0.3 for  $BA^3$  and  $BA^4$ .

## 6 Conclusion

The critical points that naturally appear in a random wavefield can be transformed by the addition of a spiral phase mask in a Fourier plane. Here, we studied these transformations experimentally by imprinting spiral phase masks with a charge  $n \in \llbracket -6; 6 \rrbracket$  to a laser beam impinging on a randomly scattering surface. In addition, these phase masks were combined with star-like amplitude masks with dihedral symmetries  $D_3$  and  $D_4$  in order to better control critical point transformations.

For a simple disk-shaped aperture carrying a single spiral mode  $n = 0$ , we experimentally demonstrated the topological

correlation existing between the critical points of the initial wavefield  $A_0$ , and the corresponding spiral transformed field  $A_n$ . A partial transformation of vortices  $V_0^-$  into maxima  $M_{+1}$  was observed as well as a transformation of maxima  $M_0$  into vortices  $V_{+1}^+$ . Vortices  $V_0^+$  were observed to either correlate with phase saddle points  $S_{+1}^p$  or with vortices of opposite sign  $V_{+1}^-$ . For this statistical bifurcation, two transformation interpretations were suggested, calling for further future analytical studies. No simple topological correlation was found between the critical points of the wavefields  $A_0$  and  $A_n$  for  $|n| > 3$ . This result could be explained by the weak influence of spiral phase masks with a charge higher than 2 in the coherence area surrounding the critical points.

Furthermore, adding centered binary amplitude masks with dihedral symmetry  $D_3$  or  $D_4$  and *Dirac-comb*-like spiral spectra (of period 3 and 4), we demonstrated that it is possible to deeply modify the topological correlation between critical points. The observed changes arise from the introduction of a periodicity in the transformation between the critical points. We could thereby extend the correlation to spiral phase masks with charges higher than 3, and reinforce some spatial correlation intrinsically present with a circular-aperture symmetry. For the amplitude mask with a  $D_3$ -symmetry, a cyclic permutation between negatively charged vortices  $V^-$ , maxima  $M$ , and positively charged vortices  $V^+$ , is observed. For the amplitude mask with a  $D_4$ -symmetry, phase saddle points participate as complementary points to complete the 4-periodic cycle. Considering the addition of 2-charged spiral masks, transpositions between  $V^-$  and  $V^+$ , and between  $M$  and  $S^p$  were also revealed for  $D_4$ -symmetry. The enhancement of the spatial correlation between the critical points of the wavefields  $A_0$  and  $A_n$  (compared to  $BA^\infty$ ) could be explained by the strong influence of the spiral phase mask in the coherence area surrounding each critical point, when the binary amplitude masks are added.

Here, cyclic permutations were controlled using binary amplitude masks enforcing periodicity. Interestingly, our study may extend to other amplitude masks with a dihedral symmetry, such as polygonal [19] and triangular apertures [25], whose interactions with vortex beams were studied in free space. For N-gons, the  $N^{\text{th}}$  spiral harmonics have a much lower amplitude than the fundamental spiral mode ( $n = 0$ ). As a result, the spatial correlations between critical points for  $|n| > 3$  is weaker than for  $BA^N$ , and vanishes with the increasing charge of the SP mask (verified in numerical simulation).

In a nutshell, we showed here that it is possible to manipulate the topological correlation between critical points and to control the transformation of critical points in random wavefields by combining amplitude masks and spiral phase transforms. Topological manipulation of critical points in random wavefields is of high importance to understand and control light propagation through scattering and complex media.

## Funding Information

This work was partially funded by the french Agence Nationale pour la Recherche (NEOCASTIP ANR-CE09-0015-01, SpeckleSTED ANR-18-CE42-0008-01).

## References

- [1] R. Horstmeyer, H. Ruan, and C. Yang, “Guidestar-assisted wavefront-shaping methods for focusing light into biological tissue,” **Nat Photon** **9**, 563–571 (2015). Review.
- [2] B. Rodenburg, M. P. J. Lavery, M. Malik, M. N. O’Sullivan, M. Mirhosseini, D. J. Robertson, M. Padgett, and R. W. Boyd, “Influence of atmospheric turbulence on states of light carrying orbital angular momentum,” **Opt. Lett.** **37**, 3735–3737 (2012).
- [3] E. Akkermans and G. Montambaux, *Mesoscopic Physics of Electrons and Photons* (2007).
- [4] S. Feng, C. Kane, P. A. Lee, and A. D. Stone, “Correlations and fluctuations of coherent wave transmission through disordered media,” **Phys. Rev. Lett.** **61**, 834–837 (1988).
- [5] I. Freund, M. Rosenbluh, and S. Feng, “Memory effects in propagation of optical waves through disordered media,” **Phys. Rev. Lett.** **61**, 2328–2331 (1988).
- [6] B. Judkewitz, R. Horstmeyer, I. M. Vellekoop, I. N. Papadopoulos, and C. Yang, “Translation correlations in anisotropically scattering media,” **Nature Physics** **11**, 684–689 (2015).
- [7] G. Osnabrugge, R. Horstmeyer, I. N. Papadopoulos, B. Judkewitz, and I. M. Vellekoop, “Generalized optical memory effect,” **Optica** **4**, 886–892 (2017).
- [8] I. Freund, “1001 correlations in random wave fields,” **Waves in Random Media** **8**, 119–158 (1998).
- [9] J. F. Nye and M. V. Berry, “Dislocations in Wave Trains,” **Proceedings of the Royal Society A: Mathematical, Physical and Engineering Sciences** **336**, 165–190 (1974).
- [10] M. Pascucci, G. Tessier, V. Emiliani, and M. Guillon, “Superresolution Imaging of Optical Vortices in a Speckle Pattern,” **Phys. Rev. Lett.** **116**, 093904 (2016).
- [11] M. Pascucci, S. Ganesan, A. Tripathi, O. Katz, V. Emiliani, and M. Guillon, “Compressive three-dimensional super-resolution microscopy with speckle-saturated fluorescence excitation,” **ArXiv abs/1710.05056v2** (2017).
- [12] M. Dennis, “Topical singularities in wave fields,” Ph.D. thesis, University of Bristol, UK (2001).

- [13] J. Nye, J. Hajnal, and J. Hannay, “Phase saddles and dislocations in two-dimensional waves such as the tides,” **Proceedings of the Royal Society of London A: Mathematical, Physical and Engineering Sciences** **417**, 7–20 (1988).
- [14] K. G. Larkin, D. J. Bone, and M. A. Oldfield, “Natural demodulation of two-dimensional fringe patterns. i. general background of the spiral phase quadrature transform,” **J. Opt. Soc. Am. A** **18**, 1862–1870 (2001).
- [15] M. R. Dennis, K. O’Holleran, and M. J. Padgett, “Chapter 5 singular optics: Optical vortices and polarization singularities,” (Elsevier, 2009), pp. 293 – 363.
- [16] J. Gateau, H. Rigneault, and M. Guillon, “Complementary speckle patterns: Deterministic interchange of intrinsic vortices and maxima through scattering media,” **Phys. Rev. Lett.** **118**, 043903 (2017).
- [17] I. Freund, N. Shvartsman, and V. Freilikher, “Optical dislocation networks in highly random media,” **Optics Communications** **101**, 247–264 (1993).
- [18] A. Ferrando, M. Zúñiga, M.-A. García-March, J. A. Monsoriu, and P. F. de Córdoba, “Vortex transmutation,” **Phys. Rev. Lett.** **95**, 123901 (2005).
- [19] N. Gao and C. Xie, “Experimental demonstration of free-space optical vortex transmutation with polygonal lenses,” **Opt. Lett.** **37**, 3255–3257 (2012).
- [20] R. W. Schoonover and T. D. Visser, “Creating polarization singularities with an  $n$ -pinhole interferometer,” **Phys. Rev. A** **79**, 043809 (2009).
- [21] Z. Li and C. Cheng, “Generation of second-order vortex arrays with six-pinhole interferometers under plane wave illumination,” **Appl. Opt.** **53**, 1629–1635 (2014).
- [22] Z. Yang, O. S. Magaña-Loaiza, M. Mirhosseini, Y. Zhou, B. Gao, L. Gao, S. M. H. Rafsanjani, G.-L. Long, and R. W. Boyd, “Digital spiral object identification using random light,” **Light: Science & Applications** **6**, e17013 EP – (2017). Original Article.
- [23] G. Xie, H. Song, Z. Zhao, G. Milione, Y. Ren, C. Liu, R. Zhang, C. Bao, L. Li, Z. Wang, K. Pang, D. Starodubov, B. Lynn, M. Tur, and A. E. Willner, “Using a complex optical orbital-angular-momentum spectrum to measure object parameters,” **Opt. Lett.** **42**, 4482–4485 (2017).
- [24] W. Zhang and L. Chen, “Encoding and decoding of digital spiral imaging based on bidirectional transformation of light’s spatial eigenmodes,” **Opt. Lett.** **41**, 2843–2846 (2016).
- [25] J. M. Hickmann, E. J. S. Fonseca, W. C. Soares, and S. Chavez-Cerda, “Unveiling a truncated optical lattice associated with a triangular aperture using light’s orbital angular momentum,” **Phys. Rev. Lett.** **105**, 053904 (2010).
- [26] G. C. G. Berkhout and M. W. Beijersbergen, “Method for probing the orbital angular momentum of optical vortices in electromagnetic waves from astronomical objects,” **Phys. Rev. Lett.** **101**, 100801 (2008).
- [27] L. Torner, J. P. Torres, and S. Carrasco, “Digital spiral imaging,” **Optics Express** **13**, 873 (2005).
- [28] I. Freund, “Amplitude topological singularities in random electromagnetic wavefields,” **Physics Letters A** **198**, 139–144 (1995).
- [29] D. Chandler, *Introduction to Modern Statistical Mechanics* (Oxford University Press, 1987).
- [30] F. Tournus, “Random nanoparticle deposition: Interparticle distances in 2D, 3D, and multilayer samples,” **Journal of Nanoparticle Research** **13**, 5211–5223 (2011).
- [31] M. S. Longuet-Higgins, “Reflection and refraction at a random moving surface. i. pattern and paths of specular points,” **J. Opt. Soc. Am.** **50**, 838–844 (1960).
- [32] I. Freund, “Optical vortices in gaussian random wave fields: statistical probability densities,” **J. Opt. Soc. Am. A** **11**, 1644–1652 (1994).
- [33] E. Ochoa and J. W. Goodman, “Statistical properties of ray directions in a monochromatic speckle pattern,” **J. Opt. Soc. Am.** **73**, 943–949 (1983).
- [34] J. E. Curtis and D. G. Grier, “Structure of optical vortices,” **Physical review letters** **90**, 133901 (2003).